

# Self-similar solutions for the dynamical condensation of a radiative gas layer

Kazunari Iwasaki<sup>1,2</sup> and Toru Tsuribe<sup>1</sup>

<sup>1</sup> Department of Earth and Space Science, Osaka University, Machikaneyama 1-1 Toyonaka, Osaka 560-0043, Japan

## ABSTRACT

A new self-similar solution describing the dynamical condensation of a radiative gas is investigated under a plane-parallel geometry. The dynamical condensation is caused by thermal instability. The solution is applicable to generic flow with a net cooling rate per unit volume and time  $\propto \rho^{-2} T$ , where  $\rho$ ,  $T$  and  $\lambda$  are density, temperature and a free parameter, respectively. Given  $\lambda$ , a family of self-similar solutions with one parameter is found in which the central density and pressure evolve as follows:  $\rho(x=0;t) / (\tau_c - t)^{-2}$  and  $P(x=0;t) / (\tau_c - t)^{-1}$ , where  $\tau_c$  is an epoch when the central density becomes infinite. For  $\lambda = 0$ , the solution describes the isochoric mode, whereas for  $\lambda = 1$ , the solution describes the isobaric mode. The self-similar solutions exist in the range between the two limits; that is, for  $0 < \lambda < 1$ . No self-similar solution is found for  $\lambda > 1$ . We compare the obtained self-similar solutions with the results of one-dimensional hydrodynamical simulations. In a converging flow, the results of the numerical simulations agree well with the self-similar solutions in the high-density limit. Our self-similar solutions are applicable to the formation of interstellar clouds (HI cloud and molecular cloud) by thermal instability.

Key words: hydrodynamics – instabilities – ISM : structure.

## 1 INTRODUCTION

Thermal instability (TI) is an important physical process in astrophysical environments that are subject to radiative cooling. Fall & Rees (1985) investigated the effect of TI caused by Bremsstrahlung on structure formation at galactic and subgalactic scales. TI also plays an important role in the interstellar medium (ISM). The ISM consists of a dense high-temperature phase (warm neutral medium, or WNM) and a clumpy low-temperature phase (cold neutral medium, or CNM), in supersonic turbulence. It is known that the ISM is thermally unstable in the temperature range between these two stable phases; that is, in the range  $T \approx 300 - 6000$  K (Ugalde & McCray 1972). Koyama & Inutsuka (2000, 2002) suggested that the structure of the ISM is provided by the phase transition that is caused by TI that occurs in a shock-compressed region.

The basic properties of TI were investigated by Field (1965), who investigated the TI of a spatially uniform gas using linear analysis for the unperturbed state in thermal equilibrium. The net cooling function per unit volume and time was assumed to be  $\propto \rho^{-2} T$ . Field (1965) showed that gas is isobarically unstable for  $\lambda < 1$  and isochorically unstable for  $\lambda < 0$ . In thermal non-equilibrium, how-

ever, where the heating and the cooling rates are not equal in the unperturbed state, the stability condition of TI is different from that in thermal equilibrium. This situation is, for example, generated in a shock-compressed region. Balbus (1986) derived a general criterion for the TI of gas in a non-equilibrium state. A flow dominated by cooling is isobarically unstable for  $\lambda > 2$  and is also isochorically unstable for  $\lambda > 1$ . Therefore, the phase with  $T \approx 300 - 6000$  K is both isobarically and isochorically unstable.

The non-linear evolution of TI has been investigated by many authors (Koyama & Inutsuka 2002; Audit & Hennebelle 2005; Hennebelle & Audit 2007; Heitsch et al. 2006; Vazquez-Semadeni et al. 2007) using multi-dimensional simulations. However, the nonlinear behaviour has only been investigated analytically by a few authors, using some simplifications in an attempt to gain a deeper insight into the nature of TI. Meerson (1989) investigated analytic solutions under the isobaric approximation. However, this approximation is valid only in the limit of short or intermediate-scale.

In this paper, a new semi-analytic model for the non-linear hydrodynamical evolution of TI for a thermally non-equilibrium gas is considered without the isobaric approximation. Once TI occurs, the density increases drastically until a thermally stable phase is reached. During this dynamical condensation, the gas is expected to lose its memory of the initial condition, and is expected to be-

<sup>2</sup> E-mail: iwasaki@vega.ess.sci.osaka-u.ac.jp

have in a self-similar manner (Zeldovich & Raizer 1967; Landau & Lifshitz 1959). In particular, in star formation, self-similar (S-S) solutions for a runaway collapse of a self-gravitating gas have been investigated by many authors (Penston 1969; Larson 1969; Shu 1977; Hunter 1977; Whitworth & Summers 1985; Boily & Lynden-Bell 1995). In this paper, S-S solutions describing dynamical condensation by TI are investigated by assuming a simple cooling rate without self-gravity. A family of S-S solutions which have two asymptotic limits (the isobaric and the isochoric modes) is presented.

In Section 2, we derive the S-S equations, and describe the mathematical characteristic of our S-S equations as well as the numerical methods. In Section 3, our S-S solutions are presented and their properties are discussed. In Section 4, the S-S solutions are compared with the results of one-dimensional numerical simulations. The astrophysical implications of the S-S solutions and the effect of dissipation are also discussed. Our study is summarized in Section 5.

2 FORMULATION

2.1 Basic equations

In this paper, we consider S-S solutions describing runaway condensation at a region where the cooling rate dominates the heating rate. The S-S solutions describe the evolution of the fluid after its memories of initial and boundary conditions have been lost during the runaway condensation. Therefore, the solutions are independent of how a cooling-dominated region forms.

A net cooling rate  $L = \dot{c} - \dot{h}$  is considered, where  $\dot{c}$  and  $\dot{h}$  are the cooling and heating rates per unit volume and time, respectively. In low-density regions, the main cooling process is spontaneous emission by collisionally excited gases. In this situation, the cooling rate is determined by the collision rate, which is proportional to  $n^2$ . Therefore, we adopt the following formula as the net cooling rate:

$$L(\rho; c_s) = \rho^2 c_s^2 \text{ erg cm}^{-3} \text{ s}^{-1}; \quad c_s = \frac{P}{\rho} \quad (1)$$

where  $P$ ,  $c_s$ , and  $\gamma$  are the pressure, sound speed, the ratio of specific heat, and a free parameter, respectively. The effects of viscosity and thermal conduction are neglected for simplicity.

The basic equations for a radiative gas under a plane-parallel geometry are the continuity equation,

$$\frac{\partial \rho}{\partial t} + \frac{\partial}{\partial x}(\rho v) = 0; \quad (2)$$

the equation of motion,

$$Dv/Dt + \frac{1}{\rho} \frac{\partial}{\partial x}(\rho c_s^2) = 0; \quad (3)$$

and the energy equation,

$$\frac{2}{1} \frac{D \ln c_s}{Dt} - \frac{D \ln \rho}{Dt} = \rho c_s^{2(\gamma-1)}; \quad (4)$$

where  $D = Dt = \partial/\partial t + v\partial/\partial x$  indicates Lagrangian time derivative.

2.2 Derivation of self-similar equations

The density increases infinitely because the net cooling rate is assumed to be  $\propto \rho^2 c_s^2$  in equation (1). The epoch at which the density becomes infinite is defined by  $t_c$ . We introduce a similarity variable  $\xi$  and assume that each physical quantity is given by the following form:

$$\begin{aligned} x &= x_0(t); \quad v(x;t) = v_0(t)V(\xi); \quad c_s(x;t) = c_0(t)X(\xi); \\ \rho(x;t) &= \rho_0(t)\rho(\xi) \quad \text{and} \quad P(x;t) = P_0(t)P(\xi); \end{aligned} \quad (5)$$

By assuming power-law time dependence of  $x_0(t) = at^n$ , where  $t = 1 - t_c/t$  and  $n = 1 - (\gamma - 1)$ , we find the following relations:

$$\begin{aligned} x_0(t) &= at^n; \quad v_0(t) = c_0(t) = \frac{na}{t_c} t^{n-1}; \\ \rho_0(t) &= \frac{n}{t_c} \rho^{2+\gamma} \frac{a^{2(\gamma-1)}}{c_0} t^n; \quad \text{and} \quad P_0(t) = \frac{\rho_0 c_0^2}{\gamma}; \end{aligned} \quad (6)$$

where  $\gamma = 1 + (3 - 2\gamma) - 1$ . Because the dimensional scale is introduced only by  $\rho_0$ , the time dependence of the physical quantities cannot be fixed. Therefore, we leave  $\rho_0$  as a free parameter.

For convenience, instead of  $\rho_0$ , we can use a parameter which is given by

$$= \frac{(2 - \gamma) \Gamma(3 - 2\gamma) \Gamma(1 - \gamma)}{\Gamma(1 - \gamma)!} \quad (7)$$

Using (7), the time dependence of  $\rho_0(t)$  and  $P_0(t)$  is given by

$$\rho_0(t) / t^{-(2-\gamma)} \quad \text{and} \quad P_0(t) / t^{(1-\gamma)} = \text{const}; \quad (8)$$

Substituting equations (5) and (6) into the basic equations (2), (3) and (4), the similarity equations are obtained as

$$(V + \xi) \frac{d \ln \rho}{d \xi} + \frac{dV}{d \xi} = \gamma; \quad (9)$$

$$(V + \xi) \frac{dV}{d \xi} + \frac{X^2 d \ln X}{d \xi} = \gamma V; \quad (10)$$

and

$$\begin{aligned} (V + \xi) \frac{2}{1} \frac{d \ln X}{d \xi} - \frac{d \ln \rho}{d \xi} \\ = \frac{2}{1} \rho^{2(\gamma-1)} X^{2(\gamma-1)}; \end{aligned} \quad (11)$$

2.3 Homologous special solutions

The similarity equations (9), (10) and (11) have homologous special solutions with a spatially uniform density and sound speed. Substituting  $\rho(\xi) = \rho_0$  and  $X(\xi) = X_0$  into the similarity equations (9), (10) and (11), one obtains

$$\frac{dV}{d \xi} = \gamma; \quad (12)$$

$$(V + \xi) \frac{dV}{d \xi} = \gamma V; \quad (13)$$

and

$$\frac{2!}{1} \rho_0 X_0^{2(\gamma-1)} = 0; \quad (14)$$

Equation (12) is integrated to give

$$V = \gamma \xi; \quad (15)$$

where  $V(\tau = 0) = 0$  is assumed. Substituting equation (15), equation (13) becomes

$$\tau(\tau - 1) = 0; \tag{16}$$

Therefore, homogeneous solutions exist for  $\tau = 0, \tau = 0$  or  $\tau = 1$ . Equation (14) gives the relation between  $\tau_0$  and  $X_0$ . For  $\tau = 0$ , the solution is given by  $\tau(\tau) = \tau_0, V(\tau) = 0$  and  $X(\tau) = X_0$ . The time dependences of density and sound speed are given by

$$\tau(\tau) = \text{const}; \text{ and } c_s(\tau) / \tau^{1-(2-\tau)}; \tag{17}$$

respectively. This is the homogeneous isochoric mode. For  $\tau > 1$ , the solution is unphysical because the sound speed is negative or complex. Therefore, no homogeneous isochoric solutions exist for  $\tau > 1$ . This fact is related to the Balbus criterion for the isochoric instability (Balbus 1986). The solution with  $\tau = 0$  indicates isothermal condensation. For  $\tau = 1$ , no S-S solutions are found except for the homogeneous solutions as shown in Section 3.

### 2.4 Asymptotic behaviour

In this subsection, the asymptotic behaviour of the S-S solutions at  $\tau \rightarrow 1$  and  $\tau \rightarrow 0$  is investigated.

#### 2.4.1 Solutions for $\tau \rightarrow 1$

Assuming that  $\tau(\tau)$  is a decreasing function of  $\tau$  and that  $\tau(\tau)$  and  $X(\tau)$  are increasing functions, equations (9), (10) and (11) become

$$\frac{d \ln \tau}{d \tau} \tau; \quad \frac{dV}{d \tau} \tau! V; \text{ and } \frac{d \ln X}{d \tau} \tau! \tag{18}$$

to the lowest order. Expanding to the next order, the asymptotic solutions are given by

$$\tau(\tau) \tau^{-1} + \tau_1^{(1)} \tau^{-1+1}; \tag{19}$$

$$V(\tau) \tau^{-1} V_1 + V_1^{(1)} \tau^{-2+1}; \tag{20}$$

and

$$X(\tau) \tau^{-1} X_1 + X_1^{(1)} \tau^{-2+1}; \tag{21}$$

where

$$\tau_1^{(1)} = \tau_1 V_1 \frac{\tau + 1}{1 - \tau!}; \tag{22}$$

$$V_1^{(1)} = \frac{1}{1 - \tau!} \tau! V_1^2 + \frac{X_1^2}{1 - \tau!} (\tau + 2!); \tag{23}$$

and

$$X_1^{(1)} = \frac{(\tau + 1)! V_1 X_1 + (\tau - 1) \tau X_1^{2(\tau-1)}}{2(1 - \tau!)}; \tag{24}$$

#### 2.4.2 Solutions for $\tau \rightarrow 0$

We expand  $\tau(\tau), V(\tau)$  and  $X(\tau)$  in the following forms:

$$\tau(\tau) \tau_0 + \tau_0^{(1)}; \quad V(\tau) \tau_0 + V_0^{(1)} \tau^{-1};$$

and

$$X(\tau) \tau_0 + X_0^{(1)}; \tag{25}$$

Substituting equations (25) into (9), (10) and (11), we obtain the following relations for coefficients:

$$V_0 = \tau_0 \text{ and } V_0^{(1)} = \frac{(\tau + 1) \tau_0^{(1)}}{(\tau + 1) \tau_0}; \tag{26}$$

The relation between  $\tau_0$  and  $X_0$  is given by

$$(\tau - 1) \tau_0 X_0^{2(\tau-1)} = 2! (\tau - 1); \tag{27}$$

The relation between  $\tau_0^{(1)}$  and  $X_0^{(1)}$  is given by

$$\frac{\tau_0^{(1)}}{\tau_0} + 2 \frac{X_0^{(1)}}{X_0} = 0; \tag{28}$$

and  $\tau_0$  is given by

$$\tau_0 = \frac{(2 - \tau) \tau_0}{\tau + 1}; \text{ where } \tau_0 = (\tau - 1) \tau_0 X_0^{2(\tau-1)}; \tag{29}$$

### 2.5 Critical point

Equations (9), (10) and (11) can be rewritten as

$$\frac{d \ln \tau}{d \tau} = \frac{I_2}{I_1}; \quad \frac{dV}{d \tau} = \frac{I_3}{I_1} \text{ and } \frac{d \ln X}{d \tau} = \frac{I_4}{I_1}; \tag{30}$$

where

$$I_1 = (V + \tau)^2 X^2; \quad I_2 = \frac{X^2}{V + \tau} g + f; \tag{31}$$

$$I_3 = X^2 g + I_1 (V + \tau) f; \tag{32}$$

$$I_4 = \frac{1}{2} \frac{X^2 (V + \tau)^2}{V + \tau} g + \frac{1}{2} f; \tag{33}$$

$$g(\tau; X) = (\tau - 1) \tau_0 X_0^{2(\tau-1)} X^{2(\tau-1)}; \tag{34}$$

and

$$f(\tau; V) = (V + \tau) \tau! V; \tag{35}$$

A singular point exists where  $I_1 = 0$  in each of the equations (30). This is the critical point ( $\tau = \tau_s$ ). In the S-S solutions which is smooth at this point, the numerators ( $I_2, I_3$  and  $I_4$ ) must vanish at  $\tau = \tau_s$ . Among four conditions  $I_1 = I_2 = I_3 = I_4 = 0$ , there are two independent conditions which are given by

$$(V + \tau)^2 = X^2 \text{ and } \frac{X^2}{V + \tau} g + f = 0; \tag{36}$$

#### 2.5.1 Topological property of the critical point

In this subsection, the topological properties of the critical point are investigated. We introduce a new variable  $s$  which is defined by  $ds = \tau d\tau$  (Whitworth & Summers 1985). The dimensionless quantities at infinitesimal distances from the critical point,  $s_s + s$ , are given by

$$Q(s_s + s) = Q_s + Q; \tag{37}$$

where  $Q = (\tau; \ln \tau; V; \ln X)$ . The subscript "s" indicates the value at the critical point. Substituting equation (37) into equations (30) and linearizing, one obtains

$$\frac{d Q_i}{ds} = A_{ij} j = s Q_j; \quad A_{ij} = \frac{\partial I_i}{\partial Q_j}; \tag{38}$$

The eigenvalues of  $A_{ij}$  provide the topological property of the critical point. The eigenequation is given by

$$\frac{1}{X_s} \frac{d^2 X_s}{ds^2} + b_1 \frac{1}{X_s} + b_2 = 0; \tag{39}$$

where

$$b_1 = -s f'(s) + 1 + 1/g + \dots + 2; \tag{40}$$

and

$$b_2 = \frac{2}{s} (1 - \frac{2}{s}) + \frac{4! + 2!}{2 + 2} + \frac{3}{2 + 1} + \dots + \frac{4! + 2!^2}{2! + 2!}; \tag{41}$$

where  $s = (1 - X_s)^{2(1-s)}$ . The degenerate solution,  $\eta = 0$ , is attributed to the homogeneous special solutions (see Subsection 2.3). Therefore, the topology is described by the two eigenvalues other than  $\eta = 0$ .

2.6 Numerical methods

In this subsection, our numerical method for solving the similarity equations (30) is described. We adopt  $s$  as an integrating variable. Using  $s$ , equations (30) are rewritten as

$$\frac{dQ_i}{ds} = I_i; \quad i = 1; 2; 3 \text{ and } 4; \tag{42}$$

which are not singular at the critical point.

The critical point is specified by  $(s_c, V_s)$  because there are four unknown quantities  $Q_s$  and two conditions, namely equations (36). Moreover, the similarity equations (42) are invariant under the transformation  $s \rightarrow m s, V \rightarrow m V, \eta \rightarrow \eta m^{2(1-s)}$  and  $X \rightarrow m X$ , where  $m$  is an arbitrary constant. Therefore, the S-S solution for  $(m s_c; m V_s)$  is the same as that for  $(s_c; V_s)$ . As one can take  $m$  in such a way that  $(s_c; V_s)$  satisfies the relation  $s_c^2 + V_s^2 = 1$ , the critical point is specified only by  $s_c$ .

Given  $s_c$ , the velocity is obtained as  $V_s = \sqrt{1 - s_c^2}$ . From equations (36),  $Q_s$  and  $X_s$  are determined. As  $X_s = V_s + s_c$  is positive, the range of  $s_c$  is  $1 - \frac{1}{2} < s_c < 1$ . The similarity equations (42) are integrated from  $s_c$  to both directions ( $s < 0$  and  $s > 1$ ) along the gradient derived from equation (38) using the fourth-order Runge-Kutta method. The position of the critical point  $s_c$  is determined iteratively by the bisection method until the solution satisfies the asymptotic behaviours (see Subsection 2.4).

3 RESULTS

3.1 Physically possible range of parameters  $(\alpha; \gamma)$

In this section, we constrain the parameter space  $(\alpha; \gamma)$  by physical properties of the flow.

3.1.1 Range of  $\alpha$

Using equation (8), the time dependences of the central density and pressure are given by

$$\rho_{00}(t) / t^{-(2-\alpha)} \text{ and } P_{00}(t) / t^{(1-\alpha)}; \tag{43}$$

where the subscript "00" indicates the value at the centre. During S-S condensation by cooling, the central density (pressure) must increase (decrease) monotonically with time. Therefore, the following two conditions are obtained:

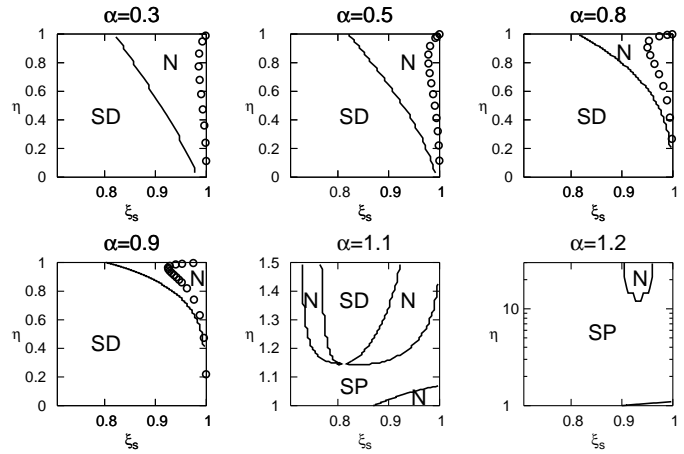


Figure 1. Topological properties of the critical point for  $\alpha = 0.3, 0.5, 0.8, 0.9, 1.1$  and  $1.2$ . The ordinates and abscissas are  $\eta$  and  $s_c$ , respectively. The letters 'N', 'SD' and 'SP' indicate a node, a saddle and a spiral, respectively. The open circles indicate S-S solutions.

$$= (2 - \alpha) < 0 \Rightarrow \alpha > 2 \tag{44}$$

and

$$(1 - \alpha) = (1 - \alpha) > 0 \Rightarrow \begin{cases} < 1 \text{ for } < 1 \\ > 1 \text{ for } > 1 \end{cases} \tag{45}$$

From equations (44) and (45), the range of  $\alpha$  is given by

$$0 < \alpha < 1 \text{ for } \alpha < 1 \\ \alpha > 1 \text{ for } \alpha > 1; \tag{46}$$

For  $\alpha = 0$ , the time dependence of  $\rho_{00}$  and  $P_{00}$  is given by

$$\rho_{00}(t) \sim \text{const.} \text{ and } P_{00}(t) / t^{1-(1-\alpha)}; \tag{47}$$

This time evolution indicates the isochoric mode. For  $\alpha = 1$ , the time dependence of  $\rho_{00}$  and  $P_{00}$  is given by

$$\rho_{00}(t) / t^{1-(2-\alpha)} \text{ and } P_{00}(t) \sim \text{const.}; \tag{48}$$

corresponding to the isobaric mode. The critical value of  $\alpha = \alpha_{eq}$  is given by the condition that the increasing rate of  $\rho_{00}(t)$  is equal to the rate of decrease of  $P_{00}(t)$ , which is given by

$$\alpha_{eq} = (2 - \alpha) = (3 - 2); \tag{49}$$

For  $\alpha = \alpha_{eq}$ , the time dependences of  $\rho_{00}$  and  $P_{00}$  are given by

$$\rho_{00}(t) / t^{1-(3-2)} \text{ and } P_{00}(t) / t^{1-(3-2)}; \tag{50}$$

Therefore, the S-S solutions for  $0 < \alpha < \alpha_{eq}$  and  $\alpha_{eq} < \alpha < 1$  are close to the isochoric and the isobaric modes, respectively.

3.1.2 The range of  $\gamma$

In the similarity equations (42), the critical point is specified by  $s_c$  for given  $\alpha$  and  $\gamma$ . The topology of the critical point is given by the two eigenvalues of the eigenequation (39) other than  $\eta = 0$ . When the two eigenvalues are real and have the same sign, the critical point is a node. When the two

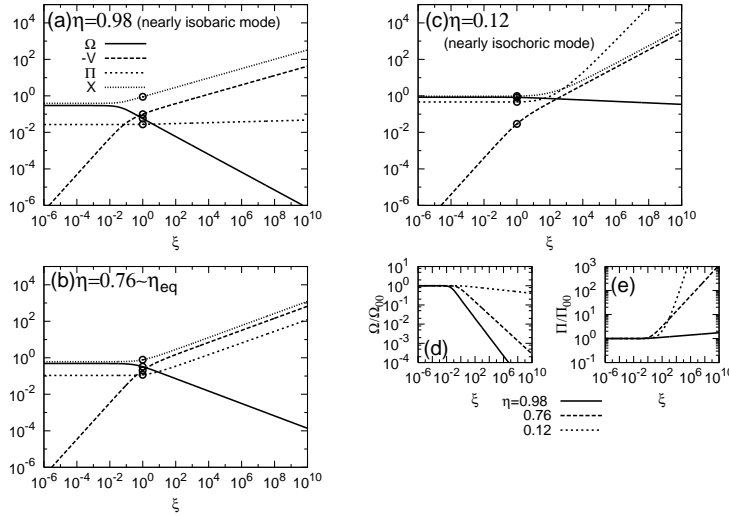


Figure 2. The distribution of dimensionless quantities ( $\Omega$ ,  $V$ ,  $\Pi$ ,  $X$ ) for (a)  $\eta=0.98$ , (b)  $0.76$  and (c)  $0.12$ . The open circles indicate the critical points. Panels (d) and (e) indicate the dependence of  $\Omega/\Omega_{00}$  and  $\Pi/\Pi_{00}$ , respectively, on  $\xi$ .

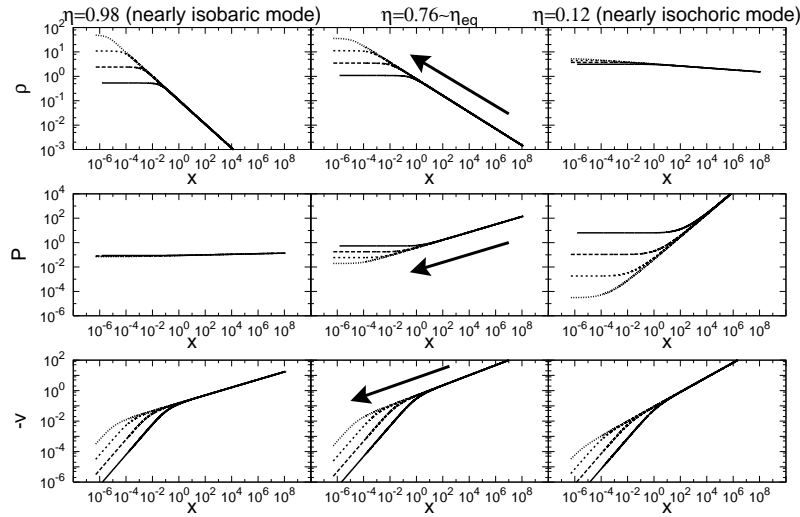


Figure 3. Time evolution of dimensional quantities ( $\rho$ ,  $P$ ,  $v$ ). The solid, long-dashed, short-dashed and dotted lines are corresponding to  $t = 1, 0.1, 0.01$  and  $0.001$ , respectively. The columns correspond to  $\eta = 0.98, 0.76$  and  $0.12$  from left to right, respectively. The arrows indicate the time evolution of  $\rho$  and  $v$ .

eigenvalues are real and have the opposite signs, the critical point is a saddle. When the two eigenvalues are complex, the critical point is a spiral. Fig. 1 shows the topology of the critical point in the parameter space  $(\eta, \beta)$  for  $\beta = 0.3, 0.5, 0.8, 0.9, 1.1$  and  $1.2$ . In Fig. 1, the letters 'N', 'SD' and 'SP' indicate a node, a saddle and a spiral, respectively. The open circles indicate the numerically obtained S-S solutions presented in Subsection 3.2. Fig. 1 shows that the topology drastically changes at  $\beta = 1$ . For  $\beta < 1$ , because the critical point is a node or a saddle, the S-S solutions are expected to exist. For  $\beta > 1$ , a non-negligible fraction of the parameter space is covered by a spiral. Almost all parameter region is a spiral for  $\beta \geq 1.2$ . We searched the S-S solutions that connect  $0 < \beta < 1$  and found them only in N and SD for  $\beta < 1$ .

### 3.2 Self-similar solutions

In this subsection, we describe new S-S solutions and investigate their properties. As shown in Subsection 3.1.1, our S-S solutions exist for  $0 < \beta < 1$  and  $\beta < 1$ .

Figs 2 (a), (b) and (c) show the obtained S-S solutions for  $\beta = 0.5$  with  $\eta = 0.98, 0.76$  and  $0.12$ , respectively. The ordinates denote the dimensionless quantities ( $\Omega$ ,  $V$ ,  $\Pi$ ,  $X$ ). The abscissas denote the dimensionless coordinate  $\xi$ . The S-S solutions for  $\eta = 0.98$  and  $0.12$  approximately represent the isobaric and the isochoric modes, respectively. The solution for  $\eta = 0.76$  corresponds to the intermediate mode shown in Subsection 3.1.1. The open circles indicate the critical points. In Figs 2 (a), (b) and (c), one can see that the S-S solutions depend strongly on  $\xi$ . Let us focus on the dependence on  $\xi$  of density and pressure, shown in Figs 2 (d) and (e), respectively. In these figures, it can be seen that, for

| $\alpha$ | $n$   | $\beta = (2 - \alpha)$ | $(1 - \alpha) = (1 - \alpha)$ | $s$    | $\rho_{00}$ | $X_{00}$ | $\rho_1$ | $V_1$   | $X_1$  |
|----------|-------|------------------------|-------------------------------|--------|-------------|----------|----------|---------|--------|
| 0.059    | 1.923 | -0.039                 | 1.882                         | 0.9999 | 0.873       | 0.977    | 0.882    | -0.0234 | 0.0408 |
| 0.272    | 1.818 | -0.181                 | 1.455                         | 0.9975 | 0.768       | 0.883    | 0.782    | -0.124  | 0.201  |
| 0.500    | 1.667 | -0.333                 | 1.000                         | 0.9907 | 0.643       | 0.766    | 0.612    | -0.244  | 0.391  |
| 0.761    | 1.493 | -0.507                 | 0.615                         | 0.9792 | 0.486       | 0.609    | 0.343    | -0.333  | 0.613  |
| 0.945    | 1.370 | -0.631                 | 0.110                         | 0.9853 | 0.360       | 0.472    | 0.123    | -0.223  | 0.805  |
| 0.995    | 1.337 | -0.663                 | 0.011                         | 0.9986 | 0.237       | 0.315    | 0.0260   | -0.0576 | 0.952  |

Table 1. Relevant parameters for obtained self-similar solutions ( $\alpha = 0.5$ ) are summarized.

$\alpha = 0.98$  (the isobaric mode), the density increases sharply towards  $\eta = 0$ , whereas the pressure is almost spatially constant. In contrast, for  $\alpha = 0.12$  (the isochoric mode), the density is almost spatially constant whereas the pressure decreases sharply towards  $\eta = 0$ .

Next, the S-S solutions are shown using the dimensional physical quantities for various  $\alpha$ . Fig. 3 shows the time evolution of  $\rho$  (first row),  $P$  (second row) and  $v$  (third row). The columns in Fig. 3 corresponds to  $\alpha = 0.98, 0.76$  and  $0.12$  from left to right. The solid, long-dashed, short-dashed and dotted lines correspond to  $t = 1, 0.1, 0.01$  and  $0.001$ , respectively. From Fig. 3, one can clearly be seen that  $\rho$  specifies how the gas condenses. In the case with  $\alpha = 0.98$  (the isobaric mode), runaway condensation occurs and the density increases in the central region, whereas the pressure is spatially and temporally constant. In the case with  $\alpha = 0.12$  (the isochoric mode), the density is spatially and temporally constant and  $P_{00}$  decreases considerably. In the case with  $\alpha = 0.76$ , the condensation occurs in an intermediate manner between the isobaric and the isochoric modes.

Relevant parameters,  $(\alpha, n, \beta = (2 - \alpha), (1 - \alpha) = (1 - \alpha), s, \rho_{00}, X_{00}, \rho_1, V_1, X_1)$ , for the S-S solutions obtained for  $\alpha = 0.5$  are summarized in Table 1.

From the above results, it is concluded that the S-S solutions are specified by  $\alpha$  and contain two asymptotic limits (the isobaric and the isochoric modes). Moreover, the parameter  $\alpha$  is related to the ratio of the sound-crossing to the cooling time-scales in the central region. Both time-scales are defined by

$$t_{\text{sound}}^{\text{cen}} = \frac{x_{\text{cen}}(t)}{c_{00}(t)} = \frac{c_{\text{cen}}}{nX_{00}} t_{\text{c}} t \quad (51)$$

and

$$t_{\text{cool}}^{\text{cen}} = \frac{P_{00}(t)}{(1 - \alpha) \rho_{00}(t)^2 c_{00}(t)^2} = \frac{1}{(1 - \alpha)n} \frac{X_{00}^{2(1 - \alpha)}}{X_{00}^2} t_{\text{c}} t; \quad (52)$$

respectively, where  $c_{00}$  is the sound speed at the centre, and the scale length  $x_{\text{cen}}(t)$  and  $c_{\text{cen}}$  are defined by

$$(x_{\text{cen}}(t); t) = (0; t) = (c_{\text{cen}}) = \rho_{00} = 0.8; \quad (53)$$

From equations (51) and (52), the ratio of the above two time-scales is obtained as

$$\frac{t_{\text{sound}}^{\text{cen}}}{t_{\text{cool}}^{\text{cen}}} = \frac{c_{\text{cen}}}{(1 - \alpha) \rho_{00} X_{00}^{2 - 3\alpha}}; \quad (54)$$

Fig. 4 shows the dependence of  $\tau$  on  $\eta$  for  $\alpha = -0.5, 0.5$  and  $0.8$ . The figure shows that  $\tau \rightarrow 0$  for  $\eta \rightarrow 1$  and  $\tau \rightarrow 1$  for  $\eta \rightarrow 0$  independent of  $\alpha$ . For  $\alpha = 1$ , because  $\rho = 1$ , the gas condenses in pressure equilibrium with its surroundings. For  $\alpha = 0$ , because  $\rho = 1$ , the pressure decreases and the density

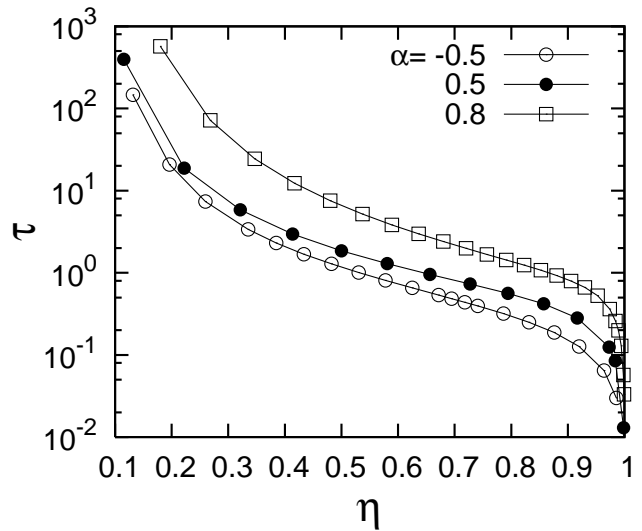


Figure 4. The dependence of  $\tau$  (equation 54) on  $\eta$ . The open circles, filled circles and open boxes indicate the S-S solutions for  $\alpha = -0.5, 0.5$  and  $0.8$ , respectively.

increases only slightly. These facts are consistent with the discussion in Subsection 3.1.1 and with Fig. 3.

Finally, we consider the range of  $\alpha$  for which the S-S solutions exist. When  $\alpha = 1.0$ , no S-S solutions are found except for the homologous special solutions (see Subsection 2.3). Moreover, as mentioned in Subsection 2.3, there are no homologous isochoric solutions for  $\alpha > 1$ . Therefore, for  $\alpha > 1$ , the condensation of the fluid is not expected to be self-similar. Fouxon et al. (2007) found a family of exact solutions for  $\alpha = 1.5 > 1$ . Their solutions are not self-similar because  $t_{\text{sound}}^{\text{cen}}$  and  $t_{\text{cool}}^{\text{cen}}$  in the central region obey the following different scaling laws:  $t_{\text{sound}}^{\text{cen}} / t^3 = 2$  and  $t_{\text{cool}}^{\text{cen}} / t$ . In their solution, during condensation, as  $t_{\text{sound}}^{\text{cen}}$  becomes much smaller than  $t_{\text{cool}}^{\text{cen}}$ , the pressure of the central region is expected to be constant and the isobaric approximation is locally valid.

#### 4 DISCUSSION

##### 4.1 Comparison with the results of time-dependent numerical hydrodynamics

We compare the S-S solutions with results of time-dependent numerical hydrodynamics using one-dimensional Lagrangian 2nd-order Godunov method (van Leer 1997). A converging flow of an initially uniform and thermal



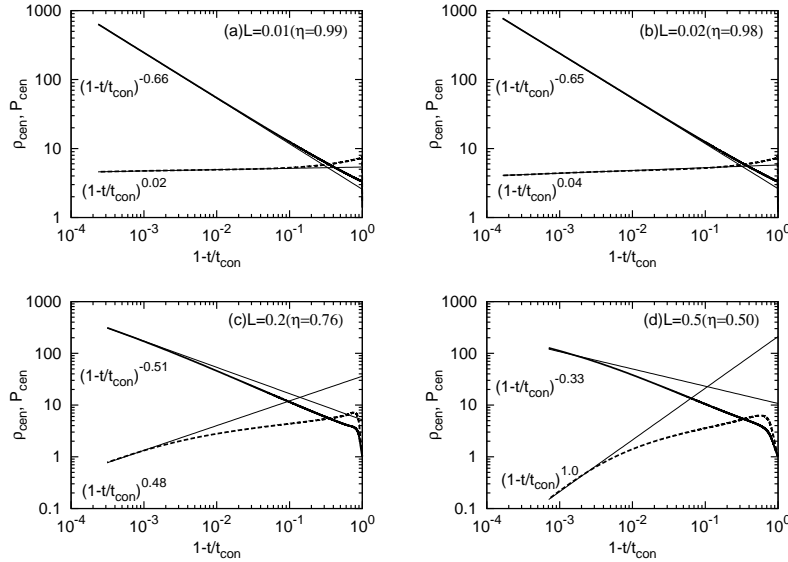


Figure 5. The time evolution of  $\rho_{00}$  (thick lines) and  $P_{00}$  (dashed lines) as a function of  $1 - t/\tau_{\text{con}}$  for (a)  $L = 0.01$ , (b)  $0.02$ , (c)  $0.2$  and (d)  $0.5$ . The thin solid lines indicate the corresponding S-S solutions.

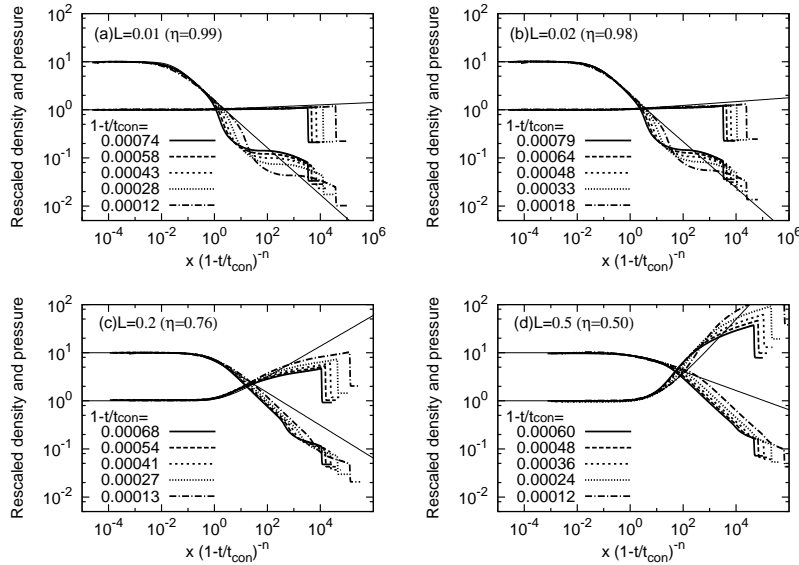


Figure 6. The distribution of the rescaled density  $(1 - t/\tau_{\text{con}})^{-2}$  and pressure  $P(1 - t/\tau_{\text{con}})^{(1) - (2)}$  as a function of scaled coordinate  $x(1 - t/\tau_{\text{con}})^{-n}$ . The  $L$  and  $\eta$  in each panel are the same as that in Fig. 5. The lines are labelled according to  $1 - t/\tau_{\text{con}}$ . The rescaled density and pressure at the centre are set to 10 and 0.1, respectively. The thin solid lines indicate the corresponding S-S solutions.

equilibrium gas ( $\rho(x) = P(x) = 1$ ), is considered. An initial velocity field is given by  $v(x) = 2 \tanh(x/L)$ , where  $L$  is a parameter. The net cooling rate is assumed to be  $L(\rho; T) = (\rho^3 - 2\rho)^{1-2} = (\rho - 1)$ , where  $\rho = 0.5$ . The inflow creates two shock waves, which propagate outward. Runaway condensation of the perturbation owing to TI occurs in the post-shock region because the cooling rate dominates the heating rate. The central density continues to grow and ultimately becomes infinite. During the runaway condensation, the inflow in the central region is expected to lose the memory of the initial and the boundary conditions, and to converge to one of the S-S solutions. The scale of perturbation

in the post-shock region can be controlled by the value of  $L$ . The larger  $L$  is, the larger the scale of perturbation becomes. We perform numerical simulations for the case with  $L = 0.005, 0.01, 0.02, 0.2$  and  $0.5$ .

Fig. 5 shows the time evolution of  $\rho_{\text{cen}}(t)$  and  $P_{\text{cen}}(t)$  as a function of  $1 - t/\tau_{\text{con}}$ , where  $\rho_{\text{cen}}$  and  $P_{\text{cen}}$  are the central density and pressure, and  $\tau_{\text{con}}$  is an epoch when  $\rho_{\text{cen}}$  becomes infinity estimated from the numerical results. The panels represent (a)  $L = 0.01$ , (b)  $0.02$ , (c)  $0.2$  and (d)  $0.5$ , respectively. Using equation (43), the time evolution of  $\rho_{\text{cen}}(t)$  and  $P_{\text{cen}}(t)$  of each simulation provides the corresponding  $n$ . As a result, the corresponding values of  $n$  are found to be

(a)0.99, (b)0.98, (c)0.76 and (d)0.50. The thin solid lines in Fig. 5 indicate the corresponding S-S solutions. From the value of  $\beta$  and Fig. 5, cases (a) and (b) correspond to the isobaric mode, case (c) corresponds to the intermediate mode ( $\beta_{eq}$ ) and case (d) corresponds to the isochoric mode. There is a difference in the convergence speed from the corresponding S-S solution. Fig. 5 shows that the convergence speed of (a) and (b) is faster than that of (c) and (d). This is because the scale-length of the condensed region of (a) and (b) is smaller and the sound-crossing time-scale is shorter.

Fig. 6 shows the time evolution of the rescaled density  $(1 - t/t_{con})^{(2)}$  and pressure  $P(1 - t/t_{con})^{(1)}$  as a function of the rescaled coordinate  $x(1 - t/t_{con})^{(1)}$ . The parameters  $L$  and  $\beta$  in Fig. 6 are the same as those in Fig. 5. The thin solid lines in Fig. 6 indicate the corresponding S-S solutions. In all the cases (a-d), the central regions are well approximated by the corresponding S-S solutions. From Fig. 6, it can be seen that the region that is well approximated by the S-S solution spreads with time in each panel.

From the above discussion, the non-linear evolution of perturbation is well approximated by one of the S-S solution in high density limit. Which S-S solution ( $0 < \beta < 1$ ) is more likely to be realised in actual environments where various scale perturbations exist? To answer this question, the dependence of  $t_{con}$  on  $L$  is investigated. Fig. 7 shows the dependence of  $1/t_{con}$  on  $1=L$ . Here,  $1=L$  and  $1/t_{con}$  correspond to the wavenumber and the growth rate of the perturbation, respectively. Therefore, Fig. 7 can be interpreted as an approximate dispersion relation for the non-linear evolution of TI. For larger  $1=L$ ,  $1/t_{con}$  is larger and  $1/t_{con}$  appears to approach a certain asymptotic value. A similar behaviour is also found in the dispersion relation of Field (1965) without heat conduction. In Fig. 7, the condensation for  $1=L = 5:0$  corresponds to the intermediate mode. Furthermore, although the isobaric condensation grows faster, there is little difference between  $1/t_{con}$  for  $1=L=200$  (the isobaric mode) and 2 (the isochoric mode). Therefore, both the isobaric and the isochoric condensations are expected to coexist in actual astrophysical environments.

4.2 Astrophysical implication

In astrophysical environment, there are roughly two ranges of temperature with  $\beta < 1$  where our S-S solutions are applicable.

In the high-temperature case,  $T \sim 2 \times 10^6 K$  (Sutherland & Dopita 1993), the dominant coolants are metal lines and Bremsstrahlung. In a shock with a velocity greater than

$$V \gtrsim 120 \text{ km s}^{-1} \frac{T}{2 \times 10^6 K}^{1/2}; \tag{55}$$

the post-shock region is thermally unstable ( $\beta < 1$ ). For example, a typical supernova satisfies this condition, and the S-S condensation is expected to occur. In reality, the density does not become infinite because the cooling time-scale increases when the gas reach the thermally stable phase. In this case, the cooled layer will rebound and overstability may take place (Chevalier & Imamura 1982; Yamada & Nishi 2001; Sutherland et al. 2003).

In the low-temperature case,  $300 < T < 6000 K$ , the dominant coolant is neutral carbon atom. Koyama & Inutsuka

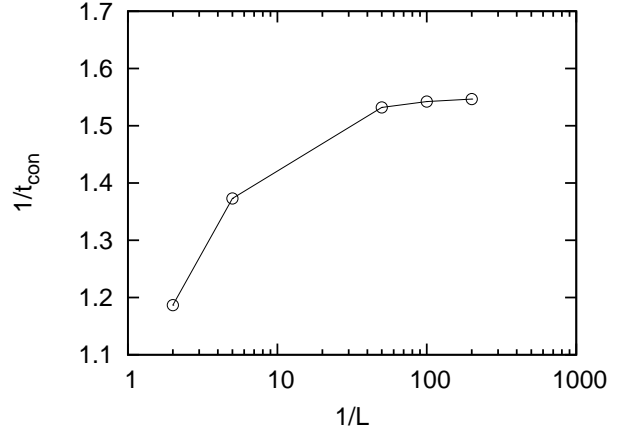


Figure 7. The dependence of the growth rate,  $1/t_{con}$ , on the wavenumber,  $1=L$ .

(2000) suggested that the structure of the ISM is caused by TI during the phase transition (WNM  $\rightarrow$  CNM). The phase transition is induced by a shock wave. Hennebelle & Perault (1999) considered the converging flow of a WNM under a plane-parallel geometry using one-dimensional hydrodynamical calculations, and investigated the condensation condition of the Mach number and pressure in the pre-shock region. In situations which satisfy their condition, S-S condensation is expected to occur.

4.3 Effects of dissipation

In the actual gas, the effect of viscosity and heat conduction becomes important on small scales. The importance of dissipation can be evaluated by the ratio between the advection and the dissipation terms, or Reynolds number, which is given by

$$R = \frac{C_v v @x T}{@x (K(T) @x T)} = \frac{C_v @0 U x_{cen}}{K(T_{00})}; \tag{56}$$

where  $C_v$ ,  $K(T)$  and  $U$  are the specific heat at constant volume, the heat conduction coefficient and the typical velocity, respectively. The Prandtl number is implicitly assumed to be of order unity. A typical length-scale is assumed to be  $x_{cen}(t)$ . If the flow converges to one of the S-S solutions, the ratio,  $R$ , between the sound-crossing and the cooling time scales is constant. Therefore  $R$  is defined by

$$R = \frac{t_{sound}^{cen}}{t_{cool}^{cen}} = x_{cen} (1 - \beta) @0 @0 C_{00}^2 @0^3; \tag{57}$$

Using  $R$ ,  $x_{cen}$  is written as

$$x_{cen} = \frac{R}{(1 - \beta) @0 @0 C_{00}^2 @0^3}; \tag{58}$$

Substituting this equation into equation (56), one obtains

$$R = \frac{C_v f_v}{(1 - \beta) @0 K_0} @0^4 @0^2; \tag{59}$$

where  $U = f_v C_{00}$  ( $f_v < 1$ ) and  $K(T_{00}) = K_0 C_{00}$ .

For the low-temperature case, we adopt  $K = 2.5 \times 10^3 \frac{\text{ergs}}{\text{cm}^2 \text{K}^2 \text{s}}$  (Parker 1953) and the following cooling function (Koyama & Inutsuka 2002):



$$(T) = 1.0 \times 10^{20} \frac{P}{T} \text{ erg cm}^{-3} \text{ s}^{-1} : \quad (60)$$

From equation (59), the Reynolds number is given by

$$R = 84 \frac{f_v}{0.1} \frac{T}{0.1} \frac{1}{10^3 K} : \quad (61)$$

In the isobaric mode,  $\beta = 0.1$  from Fig. 4. Because the Reynolds number is much larger than unity, the dynamical condensation of the post-shock region is expected to be well described by the S-S solution with  $\beta = 0.1$ .

For the high-temperature case, the cooling rate of metal lines ( $10^5 \text{ K} < T < 10^7 \text{ K}$ ) is given by

$$(T) = 2.2 \times 10^{20} T^{0.6} \text{ ergs cm}^{-3} \text{ s}^{-1} : \quad (62)$$

We adopt  $K = 1.24 \times 10^6 T^{5.2} \text{ ergs cm}^{-1} \text{ K}^{-1} \text{ s}^{-1}$  (Parker 1953). Using this formula and equation (59), the Reynolds number is given by

$$R = 85 \frac{f_v}{0.1} \frac{T}{0.1} \frac{1}{10^6 K}^{0.1} : \quad (63)$$

Because of  $R \gg 1$ , in the high-temperature case, the S-S solution with  $\beta = 0.1$  is expected to well describe the dynamical condensation.

As the temperature decreases,  $R$  decreases and becomes less than unity at a certain epoch. Thereafter, our S-S solutions are invalid and the effect of dissipation becomes important.

## 5 SUMMARY

We have provided S-S solutions describing the dynamical condensation of a radiative gas with  $\beta = 2T$ . The results of our investigation are summarized as follows:

(i) Given  $\beta$ , a family of S-S solutions written as equation (8) is found. The S-S solutions have the following two limits. The gas condenses almost isobarically for  $\beta \gg 1$ , and the gas condenses almost isochorically for  $\beta \ll 1$ . The S-S solutions exist for all values of  $\beta$  between the two limits ( $0 < \beta < 1$ ). No S-S solutions are found in  $\beta > 1$ .

(ii) The derived S-S solutions are compared with the results of numerical simulations for converging flows. In the case with any scale of perturbation in the post-shock region, our S-S solutions approximate the results of numerical simulations well in the high density limit. In the post-shock region, smaller-scale perturbations grow faster and asymptotically approach to the S-S solutions for  $\beta \gg 1$ . However, the difference of the growth rate between the isobaric mode ( $\beta_{\text{eq}} < \beta < 1$ ) and the isochoric mode ( $0 < \beta < \beta_{\text{eq}}$ ) is small. Therefore, in actual astrophysical environments, the S-S condensations for various  $\beta$  are expected to occur simultaneously.

In the S-S solutions presented in this paper, a plane-parallel geometry is assumed. This situation is much simpler than the two-dimensional simulations that are currently being carried out involving TI, so the results are of limited use, although the results may be relevant to code tests that are run on a one-dimensional simulation. The stability analysis on the present S-S solution may provide some insight into the multi-dimensional turbulent velocity field. The effect of magnetic field and self-gravity may also be important in ISM but they are neglected in this paper. These issues will be addressed in forthcoming papers.

## ACKNOWLEDGMENTS

This work is in part supported by the 21st Century COE Program "Towards a New Basic Science; Depth and Synthesis" in Osaka University, funded by the Ministry of Education, Science, Sports and Culture of Japan.

## REFERENCES

- Audit, E., & Hennebelle, P., 2005, *A & A*, 433, 1  
 Balbus, S. A., 1986 *ApJL*, 303, L79  
 Boily, C. M., & Lynden-Bell, D., 1995 *MNRAS*, 276, 133  
 Chevalier, R. A., & Imamura, J. N., 1982 *ApJ*, 261, 543  
 Dalgarno, A., & McCray, R., 1972 *ARA A*, 10, 375  
 Fall, S. M., & Rees, M. J., 1985 *ApJ*, 298, 18  
 Field, G. B., 1965 *ApJ*, 142, 531  
 Fouxon, I., Meerson, B., Asaf, M., & Livne, E., 2007 *Phys. Rev. E*, 75, 050301  
 Heitsch, F., Slyz, A. D., Devriendt, J. E. G., Hartmann, L. W., & Burkert, A., 2006, *ApJ*, 648, 1052  
 Hennebelle, P., & Audit, E., 2007, *A & A*, 465, 431  
 Hennebelle, P., & Perault, M., 1999 *A & A*, 351, 309  
 Hunter, C., 1977 *ApJ*, 218, 834  
 Koyama, H., & Inutsuka, S., 2000 *ApJ*, 532, 980  
 Koyama, H., & Inutsuka, S., 2002 *ApJL*, 564, L97  
 Landau, L. D., & Lifshitz, E. M., 1959, *Fluid Mechanics* (New York: Pergamon)  
 Larson, R. B., 1969 *MNRAS*, 145, 271  
 Meerson, B., 1989 *ApJ*, 347, 1012  
 Parker, E. N., 1953 *ApJ*, 117, 431  
 Penston, M. V., 1969 *MNRAS*, 144, 425  
 Shu, F. H., 1977 *ApJ*, 214, 488  
 Sutherland, R. S., Bicknell, G. V., & Dopita, M. A., 2003 *ApJ*, 591, 238  
 Sutherland, R. S., & Dopita, M. A., 1993 *ApJS*, 88, 253  
 van Leer, B., 1997, *J. Comput. Phys.* 135, 229  
 Vazquez-Semadeni, E., Gomez, G. C., Jappsen, A. K., Ballesteros-Paredes, J., Gonzalez, R. F., & Klessen, R. S., 2007, *ApJ*, 657, 870  
 Whitworth, A., & Summers, D., 1985 *MNRAS*, 214, 1  
 Yamada, M., & Nishi, R., 2001 *ApJ*, 547, 99  
 Zel'dovich, Y. B., & Raizer, Y. P., 1967, *Physics of Shock Waves and High-Temperature Hydrodynamic Phenomena*, ed. W. D. Hayes & R. F. Probstein (New York: Academic Press)